02

Silver centers formed in zinc-phosphate glass by femtosecond laser

© V.V. Srabionyan[1], G.Yu. Shakhgildyan[2], A.S. Lipatiev[2], M.P. Vetchinnikov[2], V.A. Durymanov[1], I.A. Viklenko[1], D.S. Rubanik[1], A.S. Mikheykin[1], A.L. Bugaev[3], L.A. Avakyan[1], V.N. Sigaev[2], L.A. Bugaev[1,¶]

[1] Faculty of Physics, Southern Federal University, Rostov-on-Don, Russia
[2] Mendeleev Russian University of Chemical Technology Moscow, Russia
[3] Paul Scherrer Institute, Villigen, Switzerland
[¶] e-mail: bugaev@sfedu.ru

Received June 01, 2025
Revised June 01, 2025
Accepted August 22, 2025

The structure of silver centers formed at different femtosecond laser direct writing speeds in zinc-phosphate glass co-doped with Ag^+ and Nd^{3+} ions was determined using X-ray absorption spectroscopy, optical absorption spectroscopy and transmission electron microscopy. It was established that at laser writing speeds from 1 to 10 μm/s, the formation of sub-nanometer nanoclusters (NCs) and predominantly small (≤ 2 nm) silver nanoparticles (NPs) occured within the laser-written tracks, with no distinct boundary observed between the sizes of NCs and NPs. A negligible number of silver NPs larger than 3–5 nm were also presented. The formation of silver NPs in the tracks was confirmed by a well-defined localized surface plasmon resonance (LSPR) band in the optical absorption spectra of these glass regions for writing speeds $\leq 10\,\mu$m/s. The dependence of the LSPR characteristics on the laser writing speed revealed that silver NPs formed at speeds $\leq 5\,\mu$m/s possess the most pronounced resonance, centered at a wavelength of ~ 450 nm. Variations in the writing speed significantly affected the LSPR intensity but only slightly shifted its spectral position, indicating the absence of both NPs aggregates and large NPs. The fraction of silver ions bounded to oxygen and the fraction of Ag atoms incorporated into silver NCs/NPs within the laser tracks were estimated. As a result of laser processing, neodymium ions remained in the Nd^{3+} state and did not form significant aggregates within the tracks. The obtained results advance the development of laser direct writing for the spatial design of plasmonic nanostructures with the determined size and agglomeration degree in glasses co-doped with plasmonic and rare-earth metal ions.

Keywords: Zinc-phosphate glass, direct recording method by femtosecond laser, silver nanoclusters/nanoparticles, localized surface plasmon resonance, local electric field.

DOI: 10.61011/EOS.2025.08.62021.8232-25

1. Introduction

Plasmonic metal centers formed in oxide glasses with embedded rare-earth (RE) ions are intensively studied, including for the development of highly efficient laser media with enhanced photoluminescence (PL) properties [1–3]. Despite significant progress in understanding the interaction mechanisms between such centers and RE ions [4,5], which lead to increased PL intensity of the latter, experimentally obtained PL enhancement for a number of oxide glasses doped with Ag, Au, and RE ions does not exceed tenfold [6–9]. Some works [10,11] have established that the mechanism of PL enhancement through the local electric field (LEF) of plasmonic nanoparticles (NPs) is dominant for particle sizes of ≥ 5 nm. Moreover, recent results have shown that for some oxide glasses there is a quantitative correspondence between the enhancement of LEF intensity near silver NP aggregates of such size and the PL intensity of Er^{3+}ions [11]. Recent studies [10] have also shown that multiple LEF enhancement near silver NP aggregates, and consequently the enhancement of PL of RE ions located in these regions, can be achieved for NPs of size ≥ 10 nm with sufficient agglomeration, whereas smaller, uniformly dispersed NPs throughout the glass volume provide only relatively small PL enhancement. These results indicate the need to develop effective experimental methods for creating plasmonic NPs of appropriate size and agglomeration degree in glasses.

To address these tasks, the direct laser writing (DLW) method, based on using focused laser pulses, appears effective and promising, allowing for precise formation of plasmonic nanostructures in glass matrices [12]. Unlike widely used thermal methods, DLW allows for the creation of two- and three-dimensional nanostructured arrays with important practical applications [13]. Experimental studies have confirmed the effectiveness of one-step synthesis of microregions with silver NPs in silicate and phosphate glasses by precise selection of femtosecond (FS) laser irradiation parameters [13].

For creating luminescent materials with plasmonic NPs and RE ions, phosphate glasses have important advantages, including low melting temperature, broad transparency range, and high solubility [14]. Phosphate glass matrices are well suited for formation and stabilization of metallic nanoclusters (NCs) and NPs, allowing tuning of optical properties by changing chemical composition [15]. Zinc-phosphate glasses of ZnO-P_2O_5(PZ) composition are of particular interest for many photonics and optoelectronic applications [16] due to their high optical transparency, thermal stability, and ability to dissolve high concentrations of transition and RE metals without crystallization. The structural flexibility of the P_2O_5-matrix, enhanced by ZnO, ensures efficient incorporation of both plasmonic NPs and RE ions, opening new possibilities for developing functional optical materials [17].

In this study, we applied the DLW method to PZ glasses doped with Ag^+ and $Nd^{3+}$for 1) studying the possibility of forming Ag NPs possessing localized surface plasmon resonance (LSPR), establishing their size distribution and agglomeration degree, 2) identifying the main types of silver centers formed under FS laser irradiation at various writing modes, 3) proposing optimal DLW regimes to obtain Ag NPs with optical and structural characteristics necessary, according to results [10], to achieve multiple enhancement of PL of RE ions. Due to difficulties in experimentally distinguishing structural differences between sub-nanometer NCs and small (≤ 2 nm) NPs in glass, the formation of such silver centers in laser tracks was studied jointly.

2. Experimental and theoretical methods

2.1. Glass synthesis and laser processing

Three types of PZ glasses were synthesized by melt quenching: PZ glass with composition $57.3ZnO-42.7P_2O_5$, PZ glass doped with Nd^{3+} ions (PZ + Nd) with composition $57.0ZnO-42.5P_2O_5-0.5Nd_2O_3$, and PZ glass co-doped with Ag^+ and Nd^{3+} (PZ+Nd+Ag) with composition $52.4ZnO-39.1P_2O_5-8.0Ag_2O-0.5Nd_2O_3$. Selection of compositions and synthesis parameters was based on previous data allowing optimization of nanostructure formation conditions [18–20]. The Nd_2O_3 ion concentration ensured uniform Nd ion distribution without clustering.

Melting was performed at 1400°C for 2 hours in an electric furnace with silicon carbide heating elements. The melt was poured into a preheated metal mold, followed by annealing at 325°C for 4 hours to relieve internal stresses.

Laser writing in polished and ground glass plates was performed with a femtosecond laser system Pharos SP (Light Conversion Ltd.) with regenerative amplification Yb:KGW operating at wavelength $\lambda = 1030 \pm 2$ nm. Pulse energy, duration, and repetition rate were 50 nJ, 180 fs and 1 MHz respectively. The laser beam was focused inside the glass plate at a depth of $\sim 162\,\mu$m below the surface using an Olympus LCPLNIR 50X objective (NA= 0.65). Laser beam polarization was oriented along the laser scanning direction. The glass sample was mounted on an air-bearing stage (Aerotech ABL1000) synchronized with the laser, allowing precise positioning and movement of the sample at various writing speeds $X = 1$, 2, 4, 5, 8, 10 and $100\,\mu$m/s). Further on, laser tracks written at these speeds are denoted (PZ+Nd+Ag).X.

2.2. Characterization of laser tracks in PZ glasses

Transmission electron microscopy with energy dispersive X-ray spectroscopy (TEM-EDX), X-ray absorption fine structure spectroscopy (XAFS), and optical absorption spectroscopy methods were used to determine the structure of silver centers in the obtained PZ glasses.

2.2.1. TEM-EDX measurements. TEM-EDX measurements were carried out using a multi-purpose electron microscope JEM-F200 (JEOL, Japan), equipped with a cold field emission electron gun operating at 200 kV acceleration voltage. TEM images were obtained at magnifications from 30000× to 400000× using condenser apertures $200\,\mu$m and $100\,\mu$m with exposure time 500−1000 ms on a high-resolution CMOS AMT camera. EDX analysis was performed with Bruker Xflash 6T/60 Quantax 400-STEM system with 4000 channels, including an XFlash energy dispersive detector cooled by Peltier, detector thickness of 0.45 mm, and operating temperature −25°C. EDX mapping and line scans were conducted using primary energy voltage 200 kV in the energy range 10 to 20 eV with a 32 s exposure, total measurement time from 6 to 10 min.

2.2.2. Optical absorption spectra measurements and processing. Optical absorption spectra of the initial glass samples were recorded in the range 290−1600 nm on a Shimadzu UV-3600 spectrophotometer. Investigation of laser tracks by bright-field microscopy was performed with an Olympus BX51 microscope equipped with a CCD camera Olympus DP73. Absorption spectra (dependence of absorption coefficient μon energy) for each laser track in the PZ glass sample series were recorded using Olympus BX51 microscope connected via quartz optical fiber to Ocean Optics USB2000 UV-Vis spectrometer. Absorption spectra of laser-modified areas were obtained using the relation $\mu^{\exp} = -\log(I_2/I_1)$, where I_1 and I_2 are the light intensities transmitted through the original glass and through the area with laser track, respectively. A 75 W xenon lamp was used as the light source.

For processing the experimental optical absorption spectrum containing features from LSPR, a developed method [21] was used. This method is based on comparing the experimental LSPR with theoretical spectra calculated for predefined structural models of interacting particles to determine their sizes. For Ag particles sized $D < 10$ nm size-dependent corrections to the dielectric function of the corresponding bulk sample were applied, calculated

according to the expression from [8]. Optical absorption spectra calculations were performed using the multi spheres T-Matrix (MSTM) Studio code [21,22], which takes into account electromagnetic interactions between particles. The fitting of parameters of the Gaussian size distribution of Ag NPs, used to calculate the theoretical optical absorption spectrum, was done by minimizing the root mean square deviation function

$$\chi^2 = \sum \left(\mu^{\exp}(\lambda_i) - \mu^{\mathrm{mod}}(\lambda_i)\right)^2,$$

where $\mu^{\exp}(\lambda_i)$ and $\mu^{\mathrm{mod}(\lambda_i)}$ are the values of the experimental and theoretical spectra, respectively, at wavelength λ_i. The contribution of nanoclusters (NCs) was modeled using a Gaussian function with fitting parameters.

2.2.3. XAFS spectra measurements and processing Near-edge fine structure of silver K-edge X-ray absorption spectra (Ag K-XANES) and extended fine structure of these spectra (Ag K-EXAFS) were measured at the CLAESS ALBA synchrotron facility (Barcelona, Spain). Powder samples were studied in transmission mode, while measurements of bulk glass plates were done in fluorescence mode. To enhance the signal from low-concentration plasmonic metal particles localized in the subsurface layer of the plates, a focused radiation beam ($\sim 100 \times 200\,\mu$m) in grazing incidence geometry along the laser track zones was used. Energy scanning at the Ag *K*-edge was performed using a Si(311) monochromator in continuous scanning mode. Higher harmonic suppression was achieved with platinum-coated mirrors.

The study of structural states of silver in the laser track regions of the PZ glass was conducted using a combined approach consisting of quantitative analysis of Ag K-XANES and subsequent processing of Ag K-EXAFS based on local silver structure models derived from XANES. Previously established high sensitivity of Ag K-XANES spectra to changes in silver local environment in oxide glasses [23] allowed inclusion of the most probable structural states of Ag in the laser track areas, capable of contributing to the XAFS spectrum formation. Fitting of experimental XANES spectra was performed with a linear combination of contributions corresponding to structural states of silver obtained from optical absorption spectra. Ag K-EXAFS spectra were processed using the Ifeffit software package [24]. The amplitude reduction factor or spectroscopic factor S_0^2(Ag−Ag) [25] for analysis of Ag−Ag bonds was determined using the spectrum of silver foil and was 0.98. Fourier transform fitting of $F(R)$ of the oscillatory part $\chi(k)$ (where$k$ is the photoelectron wave number) of the experimental EXAFS spectra was carried out in the range from $k_{\min} = 2.0\,\text{Å}^{-1}$ to $k_{\max} \sim 6.5\,\text{Å}^{-1}$. The fitting function was a linear combination of contributions corresponding to different structural states of silver identified by analyzing XANES and optical absorption spectra. The function $F(R)$, characterizing the radial distribution of silver nearest neighbors, was analyzed over an extended range of interatomic distances R (up to ~ 3.5 Å). Quantitative evaluation of fitting quality for both Ag K-XANES and EXAFS was based on minimizing the function χ^2 [26].

3. Results

3.1. TEM-EDX analysis of (PZ+Nd+Ag) glasses

TEM microphotograph of laser track in (PZ+Nd+Ag).2 glass and size distribution of formed particles are shown in Fig. 1, *a, b*. Fig. 1, *c* shows the EDX map of spatial distribution of silver and neodymium in the studied area. The particle size distribution showed predominance of small Ag NPs (including sub-nanometer Ag NCs) with sizes ≤ 2 nm alongside the presence of some larger (≥ 3 nm) particles. The EDX image indicates homogeneous distribution of Nd^{3+} ions without formation of conspicuous agglomerates.

Detailed analysis of the small size region by high-resolution TEM measurements revealed formation and growth of Ag NCs/NPs under electron beam irradiation, which appears to be a characteristic feature of PZ glasses with very strong phonon frequencies. Confirmation of this growth is illustrated in Fig. 1, *d, e*, showing evolution of Ag NPs in the (PZ+Nd+Ag).2 track by comparing microphotographs of the same spatial glass region at two consecutive times.

3.2. Optical absorption of glasses after laser writing

Before laser processing, optical absorption spectra of PZ glasses doped with silver and neodymium (PZ+Nd+Ag) contain only absorption bands characteristic for Nd^{3+} ions with no spectral features related to Ag. However, after laser writing for (PZ+Nd+Ag) samples, there is a drastic change in track coloration (compared to tracks in sample without silver (PZ+Nd)) and in absorption spectra measured in track areas. Fig. 2, *a*–*c* shows optical microphotographs of tracks written at speed $X = 1\,\mu$m/s: PZ.1, (PZ+Nd).1 and (PZ+Nd+Ag).1 along with corresponding absorption spectra. The (PZ+Nd+Ag).1 track shows a pronounced dark yellow coloration, whereas tracks in other samples are barely visible (minor yellow tint due to optical effects and camera imaging). Fig. 2, *d* compares absorption spectra in studied areas confirming formation of Ag-containing nanostructures in laser-modified zones.

Analysis of absorption spectra showed that absorption signal in laser track zones of PZ and (PZ+Nd) glasses oscillates near zero level due to interference effects in the glass substrate, indicating absence of significant absorption changes upon laser modification. In contrast, (PZ+Nd+Ag) glass exhibits a pronounced absorption band in the track zone, consistent with visual data (Fig. 1, *c*). This comparison allows concluding that optical absorption in the track zone of (PZ+Nd+Ag) glass is caused by silver nanostructures

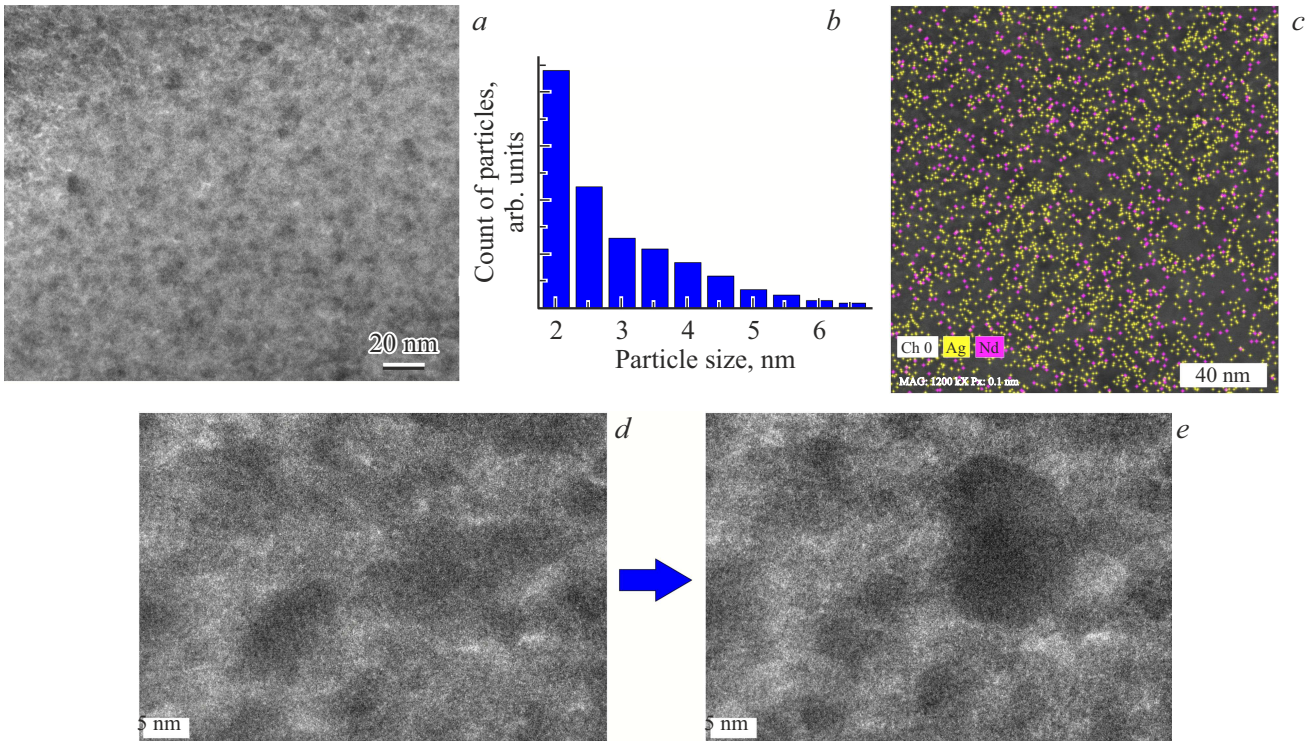

Figure 1. TEM-EDX microphotographs of laser track (PZ + Nd + Ag).2: (*a*) image demonstrating the presence of NCs/NPs Ag; (*b*) histogram of size distribution of Ag NCs/NPs obtained from image data (*a*); (*c*) EDX map of spatial distribution of Ag and Nd; (*d, e*) images of local track area recorded at two consecutive moments by high-resolution TEM.

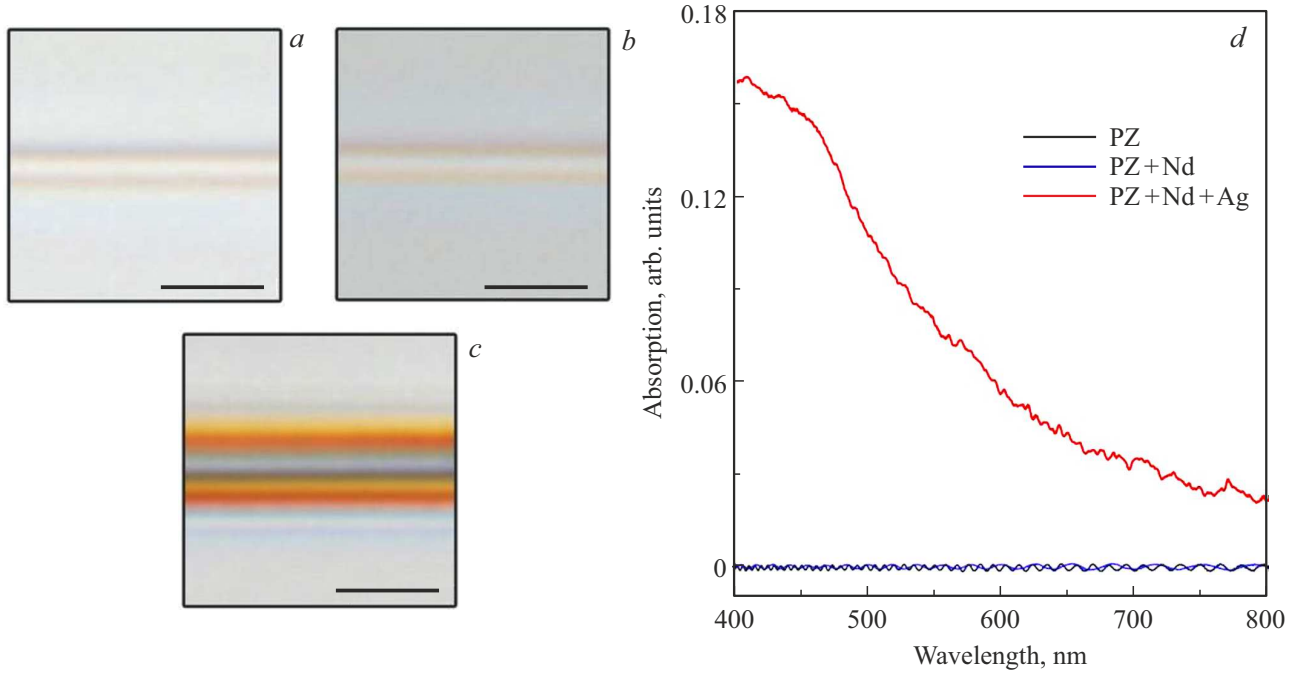

Figure 2. (a-c) Optical microphotographs (top view) of laser tracks written at speed 1 μm/s in PZ, (PZ+Nd) and (PZ+Nd+Ag) glasses. Scale bar 5 μm. (*d*) Optical absorption spectra measured in track areas presented in panels (*a*)–(*c*).

formed therein. Comparison of absorption lines of Nd^{3+} ions in (PZ+Nd) and (PZ+Nd+Ag) glasses before and after laser writing demonstrated unchanged spectral features of Nd^{3+} absorption and allowed concluding that the local environment structure of neodymium ions remains unchanged after femtosecond laser irradiation.

The influence of laser writing speed on formation of silver NCs/NPs in (PZ+Nd+Ag) glass is illustrated in Fig. 3, where parts *a* and *b* present optical absorption spectra and corresponding microphotographs of laser track areas, demonstrating decreasing absorption intensity and fading track coloration with increasing writing speed. One can see a clear dependence between laser writing speed and concentration of Ag-containing nanostructures.

Previous experimental and theoretical studies [27] indicate that the position of the LSPR maximum of Ag nanoparticles (NPs) in oxide glasses with a refractive index of $n \approx 1.5$ does not occur below 420 nm even for the smallest NP sizes, increasing with the growth of their average size, degree of agglomeration, and the refractive index of the glass matrix. Therefore, the use of the spectral range $400-800$ nm in the present work enables detection of contributions from Ag NPs of various sizes and the study of the influence of DLW parameters on their morphology and dynamics.

The experimental optical absorption spectra of (PZ+Nd+Ag) glasses shown in Fig. 3, *a* at relatively low laser writing speeds ($< 10\,\mu$m/s), measured above 400 nm wavelength, reproduce in this range the trend of the right slope of the experimental absorption centered at 350 nm for silver-doped phosphate glass at a laser writing speed of $\leq 10\,\mu$m/s [28] centered at a wavelength of 350 nm. According to the results [28], such a maximum at 350 nm is due to the absorption of silver NC. This coincidence allows concluding that at laser writing speeds $10\,\mu$m/s the absorption contribution in the track region is predominantly due to Ag NCs. The simultaneous presence of Ag NCs and NPs in the track area is confirmed by well-defined LSPR bands centered at ~ 450 nm in the same glass samples (Fig. 3, *a*). The coexistence of NCs and NPs is explained by the reduction of Ag^{+} ions during laser writing and their subsequent migration along the track, leading to formation of both NCs and NPs without a clear size boundary, resulting in the disappearance of the forbidden gap between bonding and antibonding electronic states.

Fitting of the experimental optical absorption spectra, accounting for contributions from both Ag NCs and NPs, confirmed the size distribution trend of Ag NPs obtained from TEM analysis, which shows a monotonic decrease in the number of plasmonic Ag NPs with increasing size. A similar trend was previously observed in absorption spectra of systems with ultrafine particles [29]. The absence of a clear boundary between NCs and small Ag NPs required inclusion of particles sized *D* starting from 1.0 nm in the fitting to describe the LSPR, despite the low resonance amplitude for such small particles. Note that in agglomerates containing particles of various sizes, the contribution of larger NPs dominates the formation of LSPR features even at low relative abundance, which minimizes errors related to theoretical modeling of the contribution from small particles.

The quality of fitting of optical absorption spectra is demonstrated in Fig. 3, *a* for a track written at $2\,\mu$m/s. Fig. 3, *c* and 3, *d* present the LSPR spectra of Ag NPs and their size distributions, respectively, obtained from fitting the experimental spectra in Fig. 3, *a*. It can be seen that the main differences appear in resonance amplitudes, while their positions change only slightly, since noticeable shifts (≥ 5 nm) in LSPR position can be observed with an increase in mean NP size by $\sim 20-30$ nm or with increasing particle agglomeration. Therefore, the determined NP size values from fitting the experimental optical absorption spectra based on a linear combination of contributions from NCs (modeled by Gaussian functions) and single NPs should be considered approximate. Nevertheless, the analysis suggests that decreasing writing speed leads to a monotonic increase in LSPR amplitude and Ag NP concentration, while the size distribution in Fig. 3, *d* correlates with TEM analysis data (Fig. 1, *b*) for the track zones in studied PZ glasses.

4. Ag K-XAFS-Ag analysis of silver centers in the laser track region

Experimental Ag K-XANES and EXAFS spectra measured in the laser track region (PZ+Nd+Ag).2, written at $2\,\mu$m/s, were analyzed considering three most probable Ag structural states identified also from optical absorption spectra processing: Ag–O bonds [30], NCs, and Ag NPs. Due to small differences in Ag K-XANES features between sub-nanometer clusters and small (≤ 2 nm) Ag NPs [31] and the impossibility to separate concentrations of these structural Ag states, fitting the Ag K-XANES spectrum in the laser track area (PZ+Nd+Ag).2 was done using a sum of two experimental Ag K-XANES spectra formed by contributions of Ag–O bonds (first term) and Ag–Ag bonds (second term) with corresponding weight coefficients:

$$\mu_{(\mathrm{PZ+Nd+Ag}).2}(E) = C_{\mathrm{Ag\text{–}O}}\mu_{(\mathrm{PZ+Nd+Ag})}(E) + (1 - C_{\mathrm{Ag\text{–}O}})\mu_{\mathrm{AgNCs,NPs}}(E), \quad (1)$$

where E is the X-ray photon energy, $\mu_{(\mathrm{PZ+Nd+Ag})}$ is the experimental Ag K-XANES spectrum of the powder sample of (PZ+Nd+Ag) glass not processed by DLW and thus lacking Ag NCs and NPs, $C_{\mathrm{Ag\text{-}O}}$ – is the fraction of Ag–O bonds in the laser track region (PZ+Nd+Ag).2; $\mu_{\mathrm{Ag}NCs,NPs}(E)$ is the experimental Ag K-XANES spectrum of sub-nanometer NCs and small NPs from [31]. The sum of two experimental spectra corresponding to the first and second terms in expansion (1) was performed by aligning energy positions of *K* absorption edges in experimental spectra of silver foil measured simultaneously

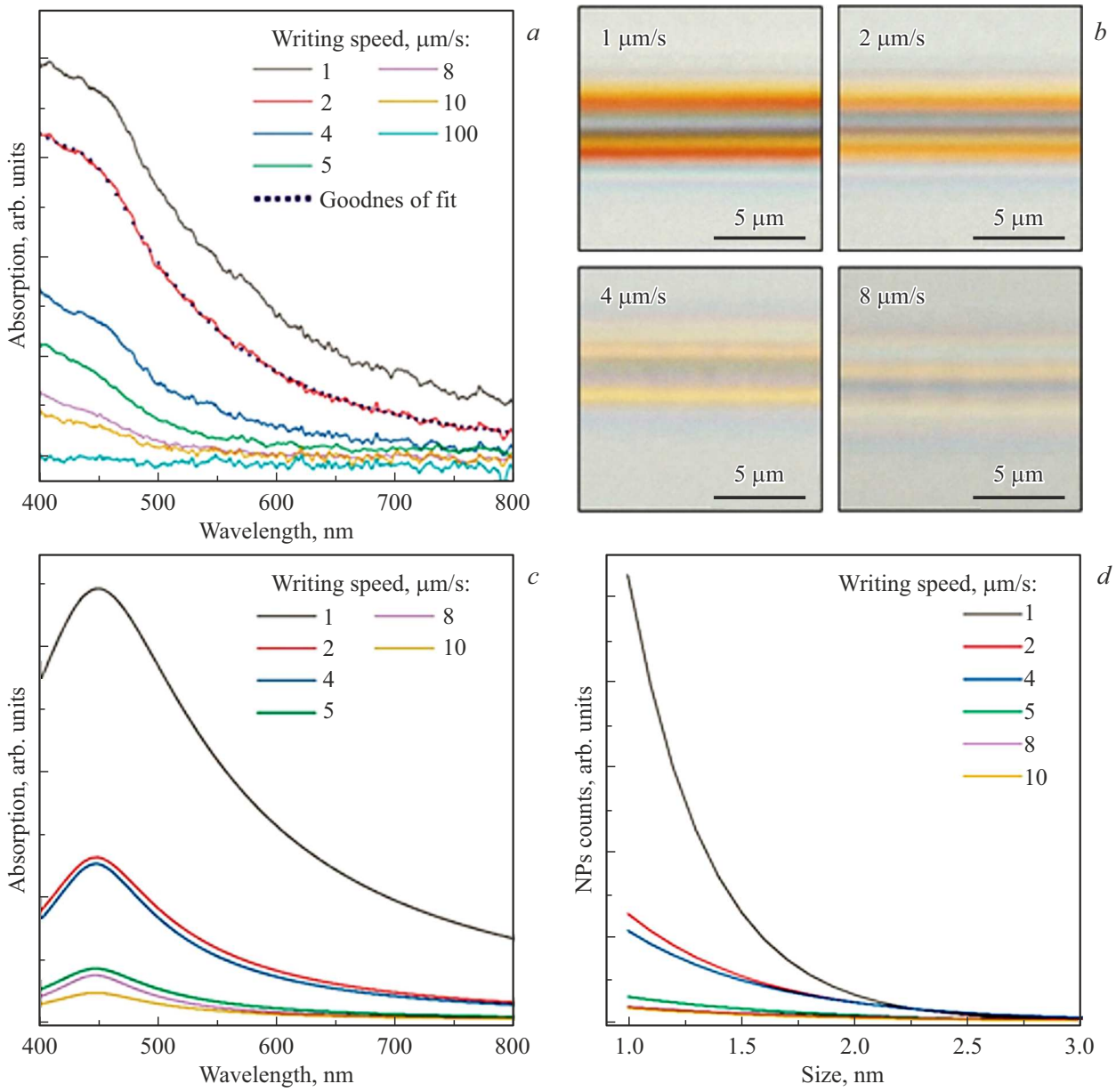

Figure 3. (*a*) Optical absorption spectra measured in laser track zones written at different speeds in (PZ+Nd+Ag) glass. Quality of fitting is illustrated by dashed curve for track written at 2 μm/s. (*b*) Optical microphotographs (top view) of tracks written in (PZ+Nd+Ag) glass at various speeds. Scale bar 5 μm. (*c*) LSPR spectra of Ag NPs extracted from experimental absorption spectra at different writing speeds shown in (*a*). (*d*) Size distribution of Ag NPs obtained by fitting LSPR spectra, showing dependence of the number and size of Ag NPs on laser writing speed.

with glass spectra. Fitting results of the experimental Ag K-XANES spectrum from the laser track region (PZ+Nd+Ag).2 by formula (1) are presented in Fig. 4, *a* along with separate contributions of the first and second terms. This fitting based on formula (1) allowed determination of the value of $C_{\text{Ag-O}} = 0.65 \pm 0.04$. The fitting quality indicator χ^2 was seven times better than when using only the first term in decomposition (1), confirming the presence of formed sub-nanometer Ag NCs and small (≤ 2 nm) Ag NPs in the laser track region (PZ+Nd+Ag).2.

To confirm results obtained from Ag K-XANES and to obtain additional parameters of silver's local environment structure, Ag K-EXAFS processing was performed by simultaneous fitting of glass spectra samples (PZ+Nd+Ag) before and after laser writing. Both spectra were processed considering contributions of Ag–O bonds, varying their amplitudes but keeping fixed the coordination number ($N = 4$) of nearest oxygen atoms around Ag ions according to [30]. For the sample after laser writing, the fitting model included a sum of Ag–O and Ag–Ag bonds contributions with adjustable weights $C_{\text{Ag-O}}$ and $(1 - C_{\text{Ag-O}})$

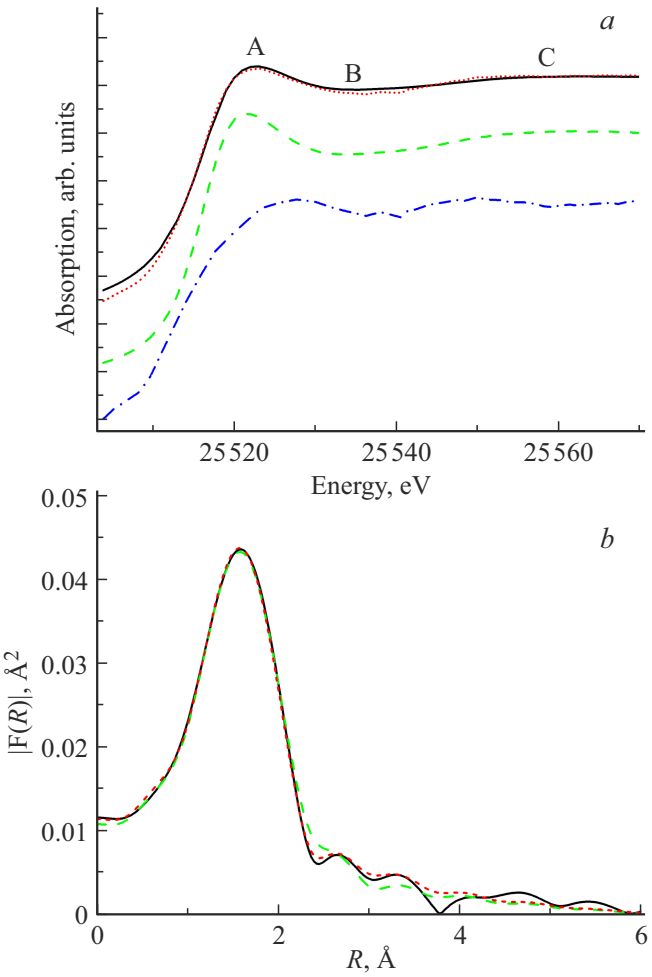

Figure 4. (a) Experimental Ag K-XANES spectra and (b) Fourier transform magnitudes $|F(R)|$ of oscillatory parts $k\chi(k)$ of experimental Ag K-EXAFS spectra and theoretical models: for laser track (PZ+Nd+Ag).2 solid black curves in panels (a, b); for (PZ+Nd+Ag) glass without laser writing (only Ag−O bonds) on panel (a) and fitting based on Ag−O-bonds only on panel (b) green dashed curves; for sub-nanometer Ag NCs and small Ag NPs from [31] on panel (a) blue dash-dot curve. Corresponding theoretical functions obtained from the fits are shown as red dotted curves in panels (a) and (b).

respectively. Common fitting parameters were: $C_{\text{Ag-O}}$, spectroscopic factor S_0^2(Ag-O), coordination number $N_{\text{Ag-Ag}}$, Debye-−Waller parameters (DW) σ^2(Ag-O), σ^2(Ag-Ag) and interatomic distances $R_{\text{Ag-O}}$, $R_{\text{Ag-Ag}}$. The fitting quality shown in Fig. 4, b, demonstrates that the model including both Ag−O and Ag−bonds reduces discrepancy χ^2 by half compared to the model including only Ag−O-bonds, confirming formation of metallic Ag NCs/NPs as a result of laser writing.

The employed fitting scheme made it possible to obtain the following additional parameters of silver local environment in the laser track area (PZ+Nd+Ag): in agreement with [30], fraction of Ag−O-bonds $C_{\text{Ag-O}} = 0.66 \pm 0.6$ close to that determined from XANES above, coordination number $N(\text{Ag-Ag}) = 5 \pm 1.5$, $\sigma^2(\text{Ag-Ag}) = 0.045$ Å^2 and average interatomic distance $R_{\text{Ag-Ag}} = 2.84$ Å, which was found to be less than the bulk silver value of 2.89 Å. Elevated values of σ^2(Ag-Ag) from room temperature measurements indicate significant distribution of interatomic distances$R_{\text{Ag-Ag}}$, explained by simultaneous presence of structurally indistinguishable sub-nanometer Ag NCs and small (≤ 2 nm) Ag NPs in glass after laser writing. Another reason for distance spread $R_{\text{Ag-Ag}}$ is its reduction for surface-layer Ag atoms in formed nanoobjects, as the proportion of such atoms increases with decreasing nanoobject size.

Data obtained from Ag K-EXAFS agree with and complement Ag K-XANES analysis results and indicate a complex nature of the silver local environment in the laser track region of (PZ+Nd+Ag) glass.

The obtained results show that varying the laser writing speed in the DLW method allows formation of silver nanoclusters/nanoparticles (NCs/NPs) in the doped PZ glass matrix. Low writing speeds ($1-4\,\mu$m/s) lead to the formation of a larger number of small Ag NPs along with a small amount of larger particles (> 5 nm). As shown in [10,11], sufficient formation of the latter is necessary for multiple enhancement of the local electric field (LEF) intensity near agglomerates of plasmonic NPs and corresponding enhancement of photoluminescence (PL) of rare-earth (RE) ions located in the vicinity of such agglomerates.

5. Conclusion

The conducted study of the structure of silver centers formed in doped PZ glass by DLW at various laser writing speeds allows the following conclusions:

– At writing speeds from 1 to 10 μm/s the laser track zones predominantly contain small Ag NPs (≤ 2 nm) and sub-nanometer Ag NCs without a distinct boundary between NC and NP sizes. There is a small number of silver NPs sized $> 3-5$ nm. At writing speed 100 μm/s Ag no Ag NCs/NPs are formed;

– The formed Ag NPs in the track region exhibit LSPR, whose intensity increases as the writing speed decreases, while its position on the wavelength scale at ~ 450 nm remains nearly unchanged, indicating minimal agglomeration of Ag NPs and absence of larger NPs sized (> 20 nm);

– At writing speed 2 μm/s about 65% of silver in the track region remains in the ionic state bonded with oxygen (Ag-O bonds), whereas 35% of Ag is present as NCs/NPs (Ag-Ag bonds). It can be expected that directly in the track zones the fraction of Ag in NCs/NPs should be higher;

– As a result of laser writing, neodymium ions in the track region of PZ glass remain in the Nd^{3+}state, not forming significant agglomerates.

The obtained results enable further development of the DLW method (for example, by subsequent thermal treatment of glasses) aimed at formation of larger Ag NPs (≥ 10 nm) with controlled particle agglomeration degree,

which is necessary to achieve multiple enhancement of intensities of both LEF near such agglomerates and PL of RE ions located in these areas.

Funding

This work was supported by the Russian Science Foundation grant (RSF Project No. 23-12-00102) at Southern Federal University.

Acknowledgments

The authors thank Prof. A.I. Frenkel (Brookhaven National Laboratory, USA) for providing Ag K-XAFS spectra of small Ag NCs and NPs, and the Shared Facilities Center „High-Resolution Electron Microscopy“ (SFU, Rostov-on-Don) for assistance with TEM-EDX investigations.

Conflict of interest

The authors declare that they have no conflict of interest.

References

[1] Q. Pan, D. Yang, G. Dong, J. Qiu, Z. Yang. Prog. Mater. Sci., **130**, 100998 (2022). DOI: 10.1016/j.pmatsci.2022.100998
[2] T. Cesca, B. Kalinic, C. Maurizio, C. Scian, G. Battaglin, P. Mazzoldi, G. Mattei. Nanoscale, **6** (3), 1716–1724 (2014). DOI: 10.1039/C3NR04108E
[3] A.S. Kuznetsov, V.K. Tikhomirov, M. V. Shestakov, V. V. Moshchalkov. Nanoscale, **5** (21), 10065 (2013). DOI: 10.1039/c3nr02798h
[4] E. Trave, M. Back, E. Cattaruzza, F. Gonella, F. Enrichi, T. Cesca, B. Kalinic, C. Scian, V. Bello, C. Maurizio, G. Mattei. J. Lumin., **197**, 104–111 (2018). DOI: 10.1016/J.JLUMIN.2018.01.025
[5] W. Zhang, J. Lin, M. Cheng, S. Zhang, Y. Jia, J. Zhao. J. Quant. Spectrosc. Radiat. Transf., **159**, 39–52 (2015). DOI: 10.1016/j.jqsrt.2015.03.002
[6] N.N. Yusof, S.K. Ghoshal, S.A. Jupri, M.N. Azlan. Opt. Mater. (Amst)., **110**, 110403 (2020). DOI: 10.1016/j.optmat.2020.110403
[7] M.P. Vetchinnikov, G.Y. Shakhgildyan, E.S. Ignat'eva, A.I. Ozerova, K.I. Runina, V.N. Sigaev. Glas. Ceram., **81** (9–10), 391–397 (2025). DOI: 10.1007/s10717-025-00716-2
[8] G. Shakhgildyan, L. Avakyan, M. Ziyatdinova, G. Atroshchenko, N. Presnyakova, M. Vetchinnikov, A. Lipatiev, L. Bugaev, V. Sigaev. J. Non. Cryst. Solids, **566**, 120893 (2021). DOI: 10.1016/j.jnoncrysol.2021.120893
[9] P. Cheng, Y. Zhou, X. Su, M. Zhou, Z. Zhou. J. Alloys Compd., **714**, 370–380 (2017). DOI: 10.1016/j.jallcom.2017.04.067
[10] V.V. Srabionyan, M.P. Vetchinnikov, D.S. Rubanik, V.A. Durymanov, I.A. Viklenko, L.A. Avakyan, E.M. Zinina, G.Y. Shakhgildyan, V.N. Sigaev, L.A. Bugaev. J. Non. Cryst. Solids, **631**, 122927 (2024). DOI: 10.1016/j.jnoncrysol.2024.122927
[11] V.V. Srabionyan, D.S. Rubanik, V.A. Durymanov, I.A. Viklenko, L.A. Avakyan, L.A. Bugaev. Opt. i spectr., **133** (4), 408–414 (2025). (in Russian) DOI: 10.61011/OS.2025.04.60538.7618-24
[12] A.I. Ignatiev, D.A. Klyukin, V.S. Leontieva, N. V. Nikonorov, T.A. Shakhverdov, A.I. Sidorov. Opt. Mater. Express, **5** (7), 1635 (2015). DOI: 10.1364/OME.5.001635
[13] G.Y. Shakhgildyan, A.S. Lipatiev, S.S. Fedotov, M.P. Vetchinnikov, S.V. Lotarev, V.N. Sigaev. Ceram. Int., **47** (10), 14320–14329 (2021). DOI: 10.1016/j.ceramint.2021.02.012
[14] U. Hoppe, G. Walter, R. Kranold, D. Stachel. J. Non. Cryst. Solids, **263–264**, 29–47 (2000). DOI: 10.1016/S0022-3093(99)00621-3
[15] I. Konidakis, A. Karagiannaki, E. Stratakis. Nanoscale, **14** (8), 2966–2989 (2022). DOI: 10.1039/D1NR07711B
[16] Y. Petit, S. Danto, T. Guérineau, A. Abou Khalil, A. Le Camus, E. Fargin, G. Duchateau, J.-P. Bérubé, R. Vallée, Y. Messaddeq, T. Cardinal, L. Canioni. Adv. Opt. Technol., **7** (5), 291–309 (2018). DOI: 10.1515/aot-2018-0037
[17] A.S. Lipat'ev, G.Y. Shakhgil'dyan, T.O. Lipat'eva, S. V. Lotarev, S.S. Fedotov, M.P. Vetchinnikov, E.S. Ignat'eva, N. V. Golubev, V.N. Sigaev, P.G. Kazanskii. Glas. Ceram., **73** (7–8), 277–282 (2016). DOI: 10.1007/s10717-016-9872-1
[18] G.Y. Shakhgildyan, M.Z. Ziyatdinova, M.P. Vetchinnikov, S.V. Lotarev, V.I. Savinkov, N.N. Presnyakova, E.V. Lopatina, G.A. Vilkovisky, V.N. Sigaev. J. Non. Cryst. Solids, **550**, 120408 (2020). DOI: 10.1016/j.jnoncrysol.2020.120408
[19] G.Y. Shakhgildyan, A.S. Lipatiev, M.P. Vetchinnikov, V.V. Popova, S.V. Lotarev, N.V. Golubev, E.S. Ignat'eva, M.M. Presniakov, V.N. Sigaev. J. Non. Cryst. Solids, **481**, 634–642 (2018). DOI: 10.1016/j.jnoncrysol.2017.12.011
[20] G.Y. Shakhgil'dyan, A.S. Lipat'ev, M.P. Vetchinnikov, V. V. Popova, S. V. Lotarev, V.N. Sigaev. Glas. Ceram., **73** (11), 420–422 (2017). DOI: 10.1007/s10717-017-9902-7
[21] L.A. Avakyan, M. Heinz, A. V Skidanenko, K.A. Yablunovski, J. Ihlemann, J. Meinertz, C. Patzig, M. Dubiel, L.A. Bugaev. J. Phys. Condens. Matter, **30** (4), 045901 (2018). DOI: 10.1088/1361-648X/aa9fcc
[22] D.W. Mackowski, M.I. Mishchenko. J. Quant. Spectrosc. Radiat. Transf., **112** (13), 2182–2192 (2011). DOI: 10.1016/j.jqsrt.2011.02.019
[23] M. Heinz, V. V. Srabionyan, A.L. Bugaev, V. V. Pryadchenko, E. V. Ishenko, L.A. Avakyan, Y. V. Zubavichus, J. Ihlemann, J. Meinertz, E. Pippel, M. Dubiel, L.A. Bugaev. J. Alloys Compd., 681, 307–315 (2016). DOI: 10.1016/j.jallcom.2016.04.214
[24] B. Ravel, M. Newville. J. Synchrotron Radiat., **12** (4), 537–541 (2005). DOI: 10.1107/S0909049505012719
[25] B.A. Manning, S.R. Kanel, E. Guzman, S.W. Brittle, I.E. Pavel. J. Nanoparticle Res., **21** (10), 213 (2019). DOI: 10.1007/s11051-019-4656-5
[26] M. Newville, B. Ravel. In: *IFEFFIT and LARCH*, 2021, pp. 791–795. DOI: 10.1107/S1574870720003407
[27] M. Heinz, V.V. Srabionyan, A.L. Bugaev, V.V. Pryadchenko, E.V. Ishenko, L.A. Avakyan, Y.V. Zubavichus, J. Ihlemann, J. Meinertz, E. Pippel, M. Dubiel, L.A. Bugaev. J. Alloys Compd., **681**, 307–315 (2016). DOI: 10.1016/j.jallcom.2016.04.214
[28] N. Marquestaut, Y. Petit, A. Royon, P. Mounaix, T. Cardinal, L. Canioni. Adv. Funct. Mater., **24** (37), 5824–5832 (2014). DOI: 10.1002/adfm.201401103

[29] V.V. Srabionyan, L.A. Avakyan, V.A. Durymanov, D.S. Rubanik, I.A. Viklenko, A.V. Skunova, L.A. Bugaev. J. Phys. Chem. Solids, **179**, 111412 (2023). DOI: 10.1016/j.jpcs.2023.111412
[30] M.P. Vetchinnikov, V.V. Srabionyan, E.M. Zinina, E.S. Ignat'eva, K.I. Runina, V.A. Durymanov, I.A. Viklenko, D.S. Rubanik, I.V. Pankov, E.V. Khramov, A.A. Veligzhanin, L.A. Avakyan, G.Y. Shakhgildyan, V.N. Sigaev, L.A. Bugaev. J. Non. Cryst. Solids, **646**, 123250 (2024). DOI: 10.1016/j.jnoncrysol.2024.123250
[31] J. Timoshenko, S. Roese, H. Hövel, A.I. Frenkel. Radiat. Phys. Chem., 175, 108049 (2020). DOI: 10.1016/j.radphyschem.2018.11.003

Translated by J.Savelyeva